Effect of Deposition Temperature and Thermal Annealing on the Properties of Sputtered NiOx/Si Heterojunction Photodiodes

Roumen Nedev , David Mateos-Anzaldo * , Eddue Osuna-Escalante , Oscar Perez-Landeros , Mario A. Curiel-Álvarez , Esteban Osorio-Urquizo , Jhonathan Castillo-Saenz , Javier Lopez-Medina , Benjamin Valdez-Salas , Nicola Nedev *

Posted Date: 3 December 2024

doi: 10.20944/preprints202412.0264.v1

Keywords: NiOx-nSi broadband photodetectors; very high responsivity; r.f. sputtering; effect of RTA treatment; light sensors

Article

Effect of Deposition Temperature and Thermal Annealing on the Properties of Sputtered NiO_x/Si Heterojunction Photodiodes

Roumen Nedev [1], David Mateos-Anzaldo [1,*], Eddue Osuna-Escalante [1], Oscar Perez-Landeros [1], Mario Curiel-Alvarez [1], Esteban Osorio-Urquizo [1], Jhonathan Castillo-Saenz [1], Javier Lopez-Medina [2], Benjamin Valdez-Salas [1] and Nicola Nedev [1,*]

[1] Instituto de Ingeniería, Universidad Autónoma de Baja California, Blvd. Benito Juárez s/n, Mexicali C.P. 21280, B.C., Mexico; roumen.nedev@uabc.edu.mx

[2] CONAHCYT Centro de Nanociencias y Nanotecnología, Universidad Nacional Autónoma de México, Ensenada C.P. 22800, Mexico; javierlo21@ens.cnyn.unam.mx

* Correspondence: dmateos@uabc.edu.mx (D.M.-A.); nicolan@uabc.edu.mx (N.N.)

Abstract: NiO_x is a p-type semiconductor with excellent stability, which make it interesting for a wide range of applications. Broadband photodetectors with high responsivity (R) were fabricated by depositing r.f. sputtered NiO_x layers on n-Si at room temperature (RT), 50 °C and 100 °C. In self-powered mode the RT diodes have R between 0.95 and 0.39 A/W for wavelengths between 365 and 635 nm, while at a reverse bias of -4V the responsivity increases to values between 22 A/W and 10.7 A/W for wavelengths in the same range. The increase of the deposition temperature leads to a decrease of R but also to a smaller reverse dark current. Thus, the 100 °C photodiodes might be more appropriate for applications where high responsivity is required, because of their smaller power consumption compared to the RT diodes. In addition, it was found that the increase of the deposition temperature leads to an increase of the diodes series resistance and the resistivity of NiO_x. The effect of Rapid Thermal Annealing (RTA) on the properties of the photodiodes was studied. Annealing at 550 °C for 6 min leads to much higher responsivity compared to R of diodes with as-deposited NiO_x. However, a disadvantage of the annealed diode is that the reverse current depends on the amplitude and polarity of previously applied bias voltage. The very high responsivity of the RTA photodiodes makes them useful as light sensors.

Keywords: NiO_x-nSi broadband photodetectors; very high responsivity; r.f. sputtering; effect of RTA treatment; light sensors

1. Introduction

NiO_x is a p-type semiconductor with excellent chemical stability and high transmittance in the visible part of the electromagnetic spectrum [1]. Its bandgap varies between 3.4 and 4.3 eV depending on the deposition technique and conditions. Due to its electrical and optical properties NiO_x is considered an attractive material for various applications, such as photovoltaic devices [2], electrochromic devices [3], gas sensors [4], ultraviolet and broadband photodetectors [5–8]. Various physical and chemical deposition techniques have been used to prepare NiO_x films. Among the most commonly used methods are sputtering [9], sol-gel spin-coating [10–12], electron beam evaporation [7] and chemical vapor deposition [13]. The structural, optical and electrical properties of the NiO_x layers depend strongly on the deposition technique. The magnetron r.f. sputtering is widely used because of the following advantages: high film quality, low density of defects, high adhesion, low cost and high deposition rate. NiO_x films have been deposited by d.c. sputtering using metallic Ni in an Ar/O_2 gas atmosphere. R.F. sputtering of NiO targets has also been studied. Despite recent advances, some challenges remain regarding the optimization of the optical and electrical properties of r.f. sputtered NiO_x layers, especially for application in photodetectors. Variations of process

 doi:10.20944/preprints202412.0264.v1

parameters such as substrate temperature, deposition power, base and working pressures affect the deposited film characteristics.

Wang et al. reported the effect of varying the deposition temperature during reactive sputtering with a fixed r.f. power of 110 W [14]. Jamal et al. studied the effect of the variation of the growth temperature in the range between room temperature (RT) and 400 °C on the properties of r.f. sputtered NiO thin films, demonstrating that increasing the substrate temperature to 100°C results in suitable properties for photovoltaic applications [15]. Ahmed et al. reported the effect of r.f. power used in the deposition and showed that the best structural, morphological and optical properties of NiO were obtained at sputtering power of 200W [16]. Elmassi et al. investigated the variation of r.f. power on structural properties of NiO thin films obtained in an O_2/Ar atmosphere, finding a relationship between power increment and crystallite size [17]. Abdur et al. investigated the impact of open-air post-annealing on the optoelectrical and structural properties of NiO films reporting that films deposited at 100°C showed favorable crystalline quality with the highest observed carrier mobility [18].

However, the results for the effect of the deposition temperature and thermal annealing processes on the properties of broadband photodetectors are limited. In this work, we study the properties of NiO_x layers deposited by r.f sputtering from a NiO target at a fixed r.f. power of 60W and temperatures between RT and 100°C. In addition, the effect of post-deposition annealing of NiO_x films on the optical and electrical properties Metal/NiO_x/nSi heterojunction diodes was studied.

2. Results

Figure 1 (a) shows the experimental dependencies of the ellipsometric parameters Ψ and Δ and the fitted curves using the Cauchy dispersion model for a NiO_x layer deposited at 100 °C and subjected to Rapid Thermal Annealing (RTA). Similar fitting results were obtained for the as-deposited layers prepared at RT, 50 °C and 100 °C and for the RTA layers deposited at the other two temperatures, RT and 50 °C. Figures 1 (b), (c) show the refractive index of the as-deposited and annealed NiO_x films. From results in Figures 1 (b) and (c) it may be concluded that the RTA process does not lead to an important change of the optical constants. The layer thicknesses, deposition rate, the refractive index (n) and the extinction coefficient (k) at 632.8 nm of the as-deposited layers are shown in Table 1. The obtained values for the optical constants n and k are close to ones reported in the literature for NiO_x [19].

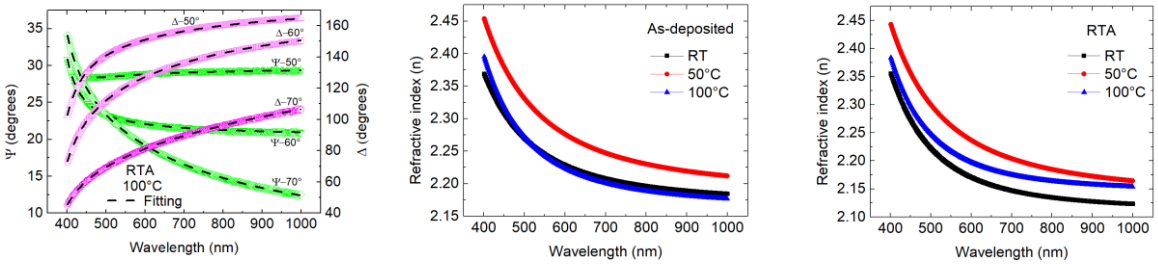

(**a**) (**b**) (c)

Figure 1. (**a**) Experimental Ψ and Δ dependences and the fitted curves for a layer deposited at 100 °C and subjected to RTA. Refractive index for: (**b**) As-deposited layers; (**c**) RTA annealed layers.

 doi:10.20944/preprints202412.0264.v1

Table 1. Thickness, deposition rate and optical constants n and k at 632.8 nm for layers deposited at the three temperatures.

Temperature (°C)	Thickness (nm)	Deposition rate (nm/min)	n	k
Room Temperature	41.5	6.92	2.25	0.03
50	48.9	8.15	2.29	0.044
100	36	6	2.25	0.01

Figure 2 (a) shows transmission spectra of a corning glass (CG) substrate and CG coated with NiO_x layers deposited at RT, 50 °C and 100 °C. The transparency of CG was ≥80% in the range of 350–1000 nm. The transmittance of the sample with NiO_x layer varies between ~60 and 80% in the visible – near IR range (400–1000 nm). Using the Tauc plot method the band gaps E_g of the films were obtained for the three deposition temperatures, 3.79, 3.82 and 3.91 eV, respectively (Figure 2 (b)). These results are in agreement with previously published values for E_g of NiO [7,19–21].

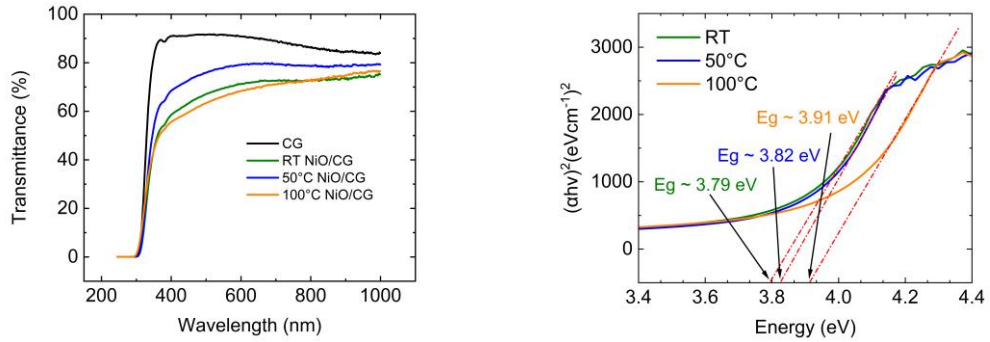

(**a**) (**b**)

Figure 2. (**a**) Transmittance of CG substrate and CG coated with NiO_x layers deposited at RT, 50 °C and 100 °C; (**b**) Band gaps of the films determined by the Tauc plot method.

Figure 3 shows current-voltage (I-V) characteristics of photodiodes with NiO_x layers deposited at RT, 50 °C and 100 °C measured by ramping the bias voltage in both directions. No hysteresis was observed in these measurements as well as after various consecutive measurements indicating low density of deep traps in the NiO_x layer and in the NiO_x/Si interfacial region. Typical rectifying dependences were measured with reverse saturation dark currents of ~3×10^{-7}, 7×10^{-7} and 1×10^{-7} A for the three deposition temperatures. Under forward bias, the current increases exponentially to voltages of ~1 V for the RT diode and to ~0.7 V for the other two diodes, and then the characteristics change their shape because of the diodes series resistance. All diodes show photoresponse under reverse bias voltages ($V_r < 0$ V) and in self-powered mode (V = 0 V). The short circuit currents (I_{SC}) under illumination with red, green, blue and UV light for the diodes with NiO_x deposited at the three temperatures are given in Table 2. The open circuit voltage (V_{OC}) depends slightly on the light intensity and varies between 0.2 V and 0.35 V depending on the light intensity and the NiO_x deposition temperature (Figure 3 (a)-(c)). The photoresponse of the diodes with NiO_x layer deposited at 100 °C is higher than that of the diodes obtained at 50 °C and is close to that of the diodes obtained at room temperature. However, an advantage of the 100 °C photodiodes is their smaller reverse dark current compared to the RT diodes.

 doi:10.20944/preprints202412.0264.v1

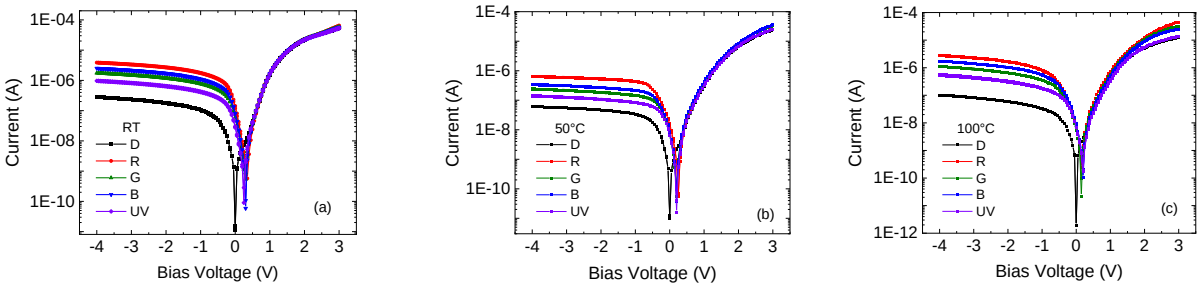

Figure 3. I-V characteristics of photodiodes with NiO_x layers deposited at: (**a**) RT, (**b**) 50 °C and (**c**) 100 °C measured in dark and under illumination with red, green, blue and UV light.

Table 2. Short circuit currents under illumination with red, green, blue and UV light for the diodes with NiO_x deposited at the three temperatures.

Light color	I_{SC} (A)		
	RT	50 °C	100 °C
Red	1.30E-07	1.50E-08	7.85E-09
Green	5.70E-08	6.70E-09	9.15E-09
Blue	7.97E-08	8.50E-09	5.25E-09
UV	2.87E-08	6.40E-09	6.85E-09

I-V characteristics of diodes with NiO_x layers deposited at the three temperatures and subjected to RTA process are shown in Figure 4. The thermal annealing leads to several important changes in the I-V dependences. Thus, the dark current and the photocurrents depend on the direction in which the bias voltage changes, leading to hysteresis at both, forward and reverse bias ramps. For forward biases, the current measured with bias increasing from 0 V towards positive voltages is smaller than the current measured in the opposite direction, most clearly seen in Figure 4 (b). The hysteresis is more pronounced under reverse biases and increases with the NiO_x deposition temperature. The reverse bias voltages at which the current reaches saturation are close to or greater than -10 V (Figure 4 (a)-(c)). The photocurrents at these large negative voltages are greater than the photocurrents of the diodes with as-deposited NiO_x layers. The highest values were obtained for the 50 °C, RTA diode (Figure 4 (b)). However, the I-V hysteresis of these photodiodes can be a disadvantage in their practical application. The inset in Figure 4 (b) shows a zoomed view of the current in the region of -0.5 – 0.5 V of a characteristic that was measured between 5 V and -10 V and then in the opposite direction. It can be seen that when ramping the bias from positive voltages towards 0 V the characteristic crosses the x-axis at positive voltage of 0.3 V, indicating increase of the negative charge trapped in the structure. In contrast, when the bias voltage varies from -10 V towards 0 V the characteristic crosses the x-axis at –0.3 V indicating increase of the positive trapped charge. Therefore, the observed hysteresis is more likely due to change of the charge state of shallow traps at the NiO_x/n-Si heterojunction interface and in the interfacial region with the bias voltage. As a result, no open circuit voltage and short circuit current were measured. Since no shift was observed of the I-V curves of diodes with as-deposited NiO_x layers it may be concluded that the RTA process has created defects, which can exchange carriers with Si, and as a result change their charge state.

 doi:10.20944/preprints202412.0264.v1

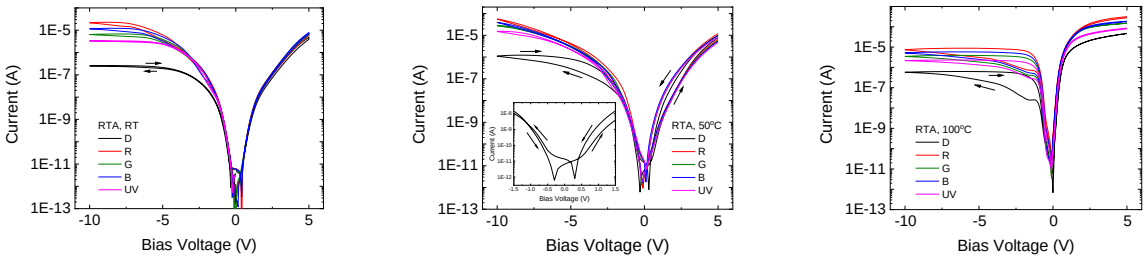

(**a**) (**b**) (**c**)

Figure 4. I-V characteristics of photodiodes with NiO_x layers deposited at: (**a**) RT, (**b**) 50 °C and (**c**) 100 °C and subjected to RTA annealing. The dependences were measured in dark and under illumination with red, green, blue and UV light.

Capacitance-Voltage (C-V) measurements were carried out in order to study in more details the effect of consecutive bias voltage ramps on the charge state of the diodes. The results in Figure 5 (a) show that ramping the voltage in both directions does not lead to hysteresis in the C-V curves of diodes with NiO_x layers deposited at the three temperatures, indicating that no charge was trapped during these measurements. In contrast, the C-V characteristics of the diodes subjected to RTA when measured under reverse bias sweep from 0 V to -10 V and back to 0 V show a displacement of the C-V curves, corresponding to increase of the trapped positive charge in the diodes (Figure 5 (b)). In accordance with the I-V measurements the diodes with NiO_x layer deposited at 50 °C showed the highest hysteresis.

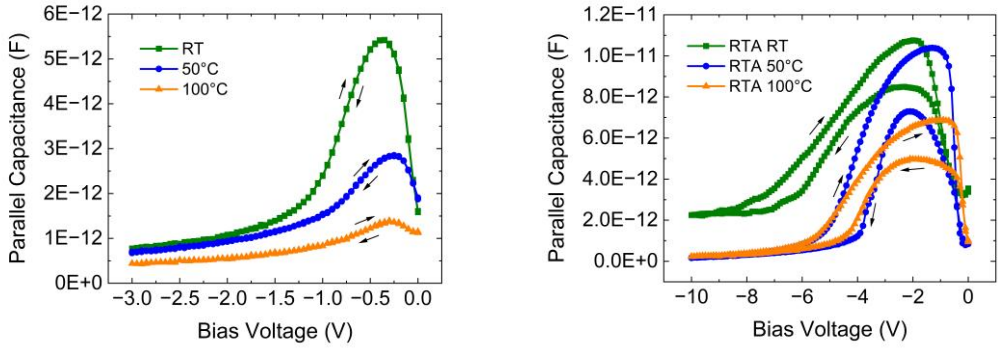

(**a**) (**b**)

Figure 5. C-V characteristics measured under reverse bias of: (**a**) Diodes with as-deposited NiO_x layers; (**b**) Diodes with RTA annealed layers.

3. Discussion

The series resistance (R_s) reduces the voltage applied on the heterojunction and thus affects the I-V characteristic. R_s can be evaluated from the slope of the I_f/g vs. I_f characteristic [22], where I_f is the forward current in the region after the exponential increase of I and g is the conductance dI_f/dV_f. In this region R_s leads to change of the shape of the I-V curve. The dependence of I/g on I may be derived by differentiating the I-V equation

$$I = I_0\left(e^{\frac{q(V-IR_s)}{nkT}} - 1\right),$$

where n is the ideality factor, which gives

$$\frac{dI}{dV} = I\frac{q}{nkT}\left(1 - R_s\frac{dI}{dV}\right),$$

or

Preprints.org (www.preprints.org) | NOT PEER-REVIEWED | Posted: 3 December 2024 doi:10.20944/preprints202412.0264.v1

$$g = I\frac{q}{nkT}(1 - R_s g),$$

By simple algebraic transformations a linear dependence of I/g on the forward current I is obtained

$$\frac{I}{g} = \frac{nkT}{q} + R_s I$$

Figure 6 (a) displays the I/g vs. I dependencies for no annealed diodes with NiO_x layers deposited at RT, 50 °C and 100 °C. The slope of the straight lines increases with the deposition temperature, indicating that R_s also increases. Since the resistivity of the n-type region of the heterojunction, n-Si, is constant it may be concluded that the increase of the deposition temperature leads to an increase of the resistivity of the NiO_x layers. Similar effect of increased resistivity was observed at a constant deposition temperature with increase of the r.f. power [23,24].

The dependence of the forward current on the voltage sweep direction makes it impossible to evaluate the series resistances of the diodes after RTA. An approximate estimation was obtained for the RTA diode with NiO_x layer deposited at RT (Figure 4 (a)) by using the I-V characteristic measured from 0 V towards positive voltages. The obtained result is compared with the I/g vs. I dependence for a no annealed diode with NiO_x layer deposited at 100 °C, the one with the highest R_s (Figure 6 (b)). The line slopes in Figure 6 (b) indicate that the RTA process leads to comparable or even higher values of R_s than those of the 100 °C diodes.

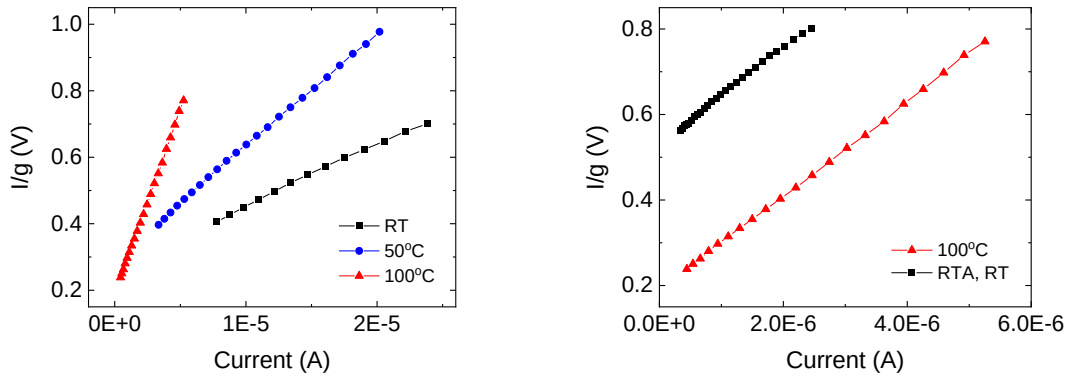

(**a**) (**b**)

Figure 6. (**a**) I/g vs. I dependencies for diodes with as-deposited NiO_x layers prepared at RT, 50 °C and 100 °C. Higher line slope corresponds to higher R_s; (**b**) Comparison of the I/g vs. I dependences for a diodes with as-deposited NiO_x prepared at 100 °C (red line) and a RTA annealed diode with NiO_x layer deposited at RT (black line); Note the difference in x-axis scale.

The responsivity (R) of the fabricated photodiodes was calculated from [25]

$$R = \frac{I_{ph}}{P_\lambda \cdot A}$$

where $I_{ph} = I_{light} - I_{dark}$ is the photocurrent, P_λ is the incident optical power at a specific wavelength λ and A is the area of the top contact. High responsivity was determined for the no annealed photodiodes. The results are shown in Figure 7 (a) and in Table 3. The responsivity of the diodes with NiO_x layer deposited at RT is higher than R of the other diodes in self-powered mode, as well as at reverse bias of -4 V. For applications where self-biased mode of operation is required, the RT diodes are the most appropriate. However, for some applications where higher responsivity is required the 100 °C photodiodes may be better option because of their smaller dark current at -4 V and R, which is close to that of the RT diode. The responsivity of the diodes subjected to RTA under V_r = -10 V is shown in Figure 7 (b). Very high values for R were determined under bias voltage of -10 V, much higher than the ones reported in the literature for broadband photodetectors. While the R of the RTA,

Preprints.org (www.preprints.org) | NOT PEER-REVIEWED | Posted: 3 December 2024 doi:10.20944/preprints202412.0264.v1

50 °C diode is the highest one this diode can be less appropriate because of it's higher dark current and lack of saturation of the photocurrent even at reverse bias voltage of -10 V. Although the RTA annealed diodes may not be appropriate for applications where precise measurement of the optical power is required, they may be useful as light sensors because of their high responsivity.

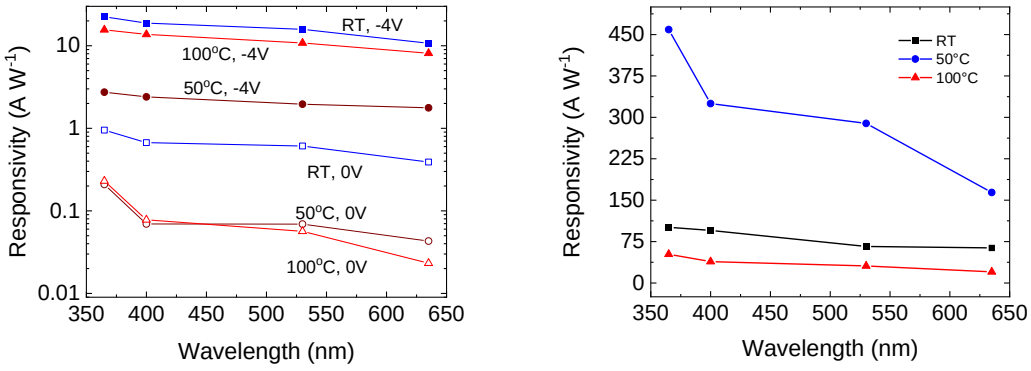

(**a**) (**b**)

Figure 7. Responsivity of photodiodes with: (**a**) As-deposited NiO_x layers; (**b**) RTA annealed NiO_x layers.

Table 3. Responsivity of photodiodes with as-deposited NiO_x layers.

Wavelength (nm)	R (A/W), Self-powered mode			R (A/W), V_r = -4 V		
	RT	50 °C	100 °C	RT	50 °C	100 °C
365	0.95	0.21	0.23	22.4	2.74	15.6
400	0.67	0.072	0.077	18.8	2.4	13.7
530	0.61	0.072	0.056	15.8	1.96	10.8
635	0.39	0.045	0.023	10.7	1.77	8.1

The obtained results for R at 0 V and at -4 V for photodiodes with as-deposited NiO_x layers are compared with results reported in the literature in Table 4. The determined responsivity of the photodiodes deposited at RT and 100°C are among the highest reported and are comparable with results published by other authors. Ma et. al. reported a responsivity of 15.8 A/W at -5V, which is slightly higher than our result for 100 °C diodes, however the maximum bias voltage used here was -4V.

Another relevant parameter is the specific detectivity (D*), which can be defined as the sensibility of a photodiode to detect weak light signals. D* involves the R at a given wavelength of the excitation light, the elementary charge (q) and the dark current density (J_D) and is given by

$$D^* = \frac{R_\lambda}{\sqrt{2qJ_D}}$$

The values obtained for the detectivity are close to the best values reported in the literature for NiO_x based photodetectors (Table 4).

Table 4. Comparison of NiO-based photodiode parameters reported in literature.

Device	Responsivity (A/W)	D (Jones)	Id (A)	On/Off Ratio	τr, τf (s)	Year [Ref.]
p-NiO/nSi	4.8×10^{-3} (at 318 nm)	-	-	-	-	2015 [26]
p-NiO/nSi	1.73, 1.81, 2.07 (at 5V, 365, 625, 850nm)	-	-	31, 35, 41 (at 5V, 365, 625, 850nm)	$3.49/7.68 \times 10^{-3}$	2022 [27]

 doi:10.20944/preprints202412.0264.v1

NiO/TiO_2	0.074 (at 0V, 380nm)	-	10^{-9}	922	$33.6/92.6 \times 10^{-3}$	2022 [28]
p-NiO/n-Si	0.95, 0.67, 0.61, 0.39 (at 0 V, 365, 400, 530, 635 nm, PRF = 60 W)	5.5×10^{10} (at 0 V, 365 nm,	8.5×10^{-12} (at 0 V)	3.4×10^{3} (at 0 V, 365 nm, PRF = 60 W)	< 0.1	2023 [24]
	22.4, 18.8, 15.8, 10.7 (at -4 V, 365, 400, 530, 635 nm)		2.8×10^{-7} (at -4 V)			
p-NiO/n-GaN	3.11×10^{-3} (at 0V)	8.69×10^{9}	-	-	$2/47 \times 10^{-3}$	2024 [29]
NiO/Ga_2O_3	5.08×10^{-3} (at -10V, 254nm)	3.19×10^{11}	2.76×10^{-12}	802.53	$62/67 \times 10^{-3}$	2024 [9]
$NiO/Al_2O_3/n$-Si	15.8 (at -5V, 365nm)	1.14×10^{14}	0.279×10^{-6}	-	$0.08/0.184 \times 10^{-3}$	2024 [30]
p-NiO/n-Si (100°C)	15.6 (at -4V, 365nm)	8.41×10^{10} (at -4V, 365nm)	1.02×10^{-7}	68.23×10^{-3}	-	This work
	0.23 (at 0V, 365nm)	2.875×10^{11} (at 0V, 365nm)	1.9×10^{-12}	3.66×10^{-3}	-	

4. Materials and Methods

NiO_x thin films were deposited on n-type (100) Si wafers with resistivity of 4–10 Ω·cm by R.F. magnetron sputtering at 25 °C (RT), 50 °C and 100 °C. The deposition time was 6 min for the three temperatures. Prior to deposition, the substrates were cleaned in an ultrasonic bath for 5 minutes with acetone, isopropyl alcohol and deionized water and dried with high-purity nitrogen. NiO target (99.9%) with dimensions of 50.8 × 3.175 mm at a working distance of 7 cm was used for deposition. The sputtering gas was ultra-high-purity (UHP) argon (99.9999%). The chamber base pressure was 1×10^{-5} Torr, the working pressure was 5 mTorr and the Ar flow was 18.9 sccm. Before the deposition the target was pre-sputtered for 20 minutes. To study the effect of thermal annealing, half of the samples were subjected to RTA process in an UHP N_2 atmosphere. The annealing was performed in a horizontal tube furnace (Zhengzhou CY Scientific Instrument Co.) equipped with a sliding rail. The N_2 flow rate was maintained at 100 mL/min, and the samples were annealed at 550 °C for 6 minutes. Following the annealing process, the samples were allowed to cool to room temperature under the same N_2 environment to ensure controlled conditions. For electrical characterization semitransparent Au electrodes (~50 nm of thickness) with area of 95 × 95 μm² spaced by 30 μm, were thermally evaporated through a shadow mask as top contacts. Aluminum with a thickness of ~300 nm was used as back contact.

The thickness and the optical constants, refractive index and extinction coefficient, were determined by ellipsometric measurements using Variable Angle Spectroscopic Ellipsometer J.A. Woollam M – 2000U. The measurements were carried out at three angles of incidence in the range of 50° - 70°. The experimental results for the ellipsometric angles Ψ and Δ were fitted in the 400 – 1000 nm range using the Cauchy dispersion model. Electrical characterization was carried out by Keithley 4200-SCS Semiconductor Characterization System. I-V dependencies were measured in dark and under illumination with red, green, blue and UV light emitting diodes (LEDs). The LEDs optical powers are given in Table 5. C-V characteristics were measured in dark at frequency of 100 kHz using a test signal with amplitude of 30 mV. The bias sweep delay time and hold time for the I-V and C-V measurements were 0.5 s and 1 s, respectively, while the voltage steps used were 50 or 100 mV.

Table 5. Optical power of the light emitting diodes used in this study.

Color	Photon wavelength/energy (nm/eV)	Optical power (mW/cm²)
Red	635/1.95	3.71
Green	530/2.34	1.03
Blue	400/3.10	1.31

 doi:10.20944/preprints202412.0264.v1

UV	365/3.40	0.335

5. Conclusions

Photodetectors with high responsivity in self-powered mode and at reverse bias of -4 V were fabricated by depositing r.f. sputtered NiO_x layers on n-Si at RT, 50 °C and 100 °C. The increase of the deposition temperature leads to a decrease of R at V = 0 V and V_r = -4 V but also to a smaller dark current at reverse biases. In addition, higher deposition temperature leads to an increase of the diodes series resistance and of the NiO_x resistivity. The diodes fabricated after RTA annealing show much higher R compared to those with as-deposited layers. A disadvantage of these diodes is the dependence of their dark current and photocurrents on the direction of the bias voltage change. As a result, the annealed diodes may be inappropriate for applications where exact determination of the optical power is required but because of the very high responsivity, they might be useful as light sensors.

References

1. Napari, M.; Huq, T.N.; Hoye, R.L.Z.; MacManus-Driscoll, J.L. Nickel oxide thin films grown by chemical deposition techniques: potential and challenges in next-generation rigid and flexible device applications. *InfoMat* **2021**, *3*, 536–576.
2. Aivalioti, C.; Manidakis, E.G.; Pelekanos, N.T.; Androulidaki, M.; Tsagaraki, K.; Viskadourakis, Z.; Spanakis, E.; Aperathitis, E. Niobium-doped NiO as p-type nanostructured layer for transparent photovoltaics. *Thin Solid Films* **2023** *778* 139910
3. Wang, F.; Zhang, W.; Jia, J.; Chen, Y.; Chen, Z.; Wang, Z.; Zhang, L.; Ma, H. Improvement of electrochromic properties of NiO film doped with ZnO prepared by magnetron sputtering. *J. Mater. Sci. Mater. Electron* **2024**, *35*,455.
4. Li, C.; Choi, P.G.; Kim, K.; Masuda, Y. High performance acetone gas sensor based on ultrathin porous NiO nanosheet. *Sens. Actuat. B-Chem* **2022**,*367*,132143.
5. Peng, Y.; Jiang, D.; Zhao, M.; Duan, Y.; Wei, H.; Li, H.; Liang, Q.; Wang, S. High-performance UV–visible photodetectors based on ZnO/perovskite heterostructures. *J. Alloys Compd.* **2023**, *965*,171372.
6. Chen, L.; Wang, Y.; Zhang, J.; Chen, L.; Zhai, J.; Song, J. Inorganic Semiconductor-Based Flexible UV Photodetector Arrays Achieved by Specific Flip-Chip Bonding. *ACS Appl. Mater. Interfaces* **2024**, *16*, 51089–51096.
7. Castillo-Saenz, J.R.; Nedev, N.; Valdez-Salas, B.; Bernechea, M.; Martínez-Guerra, E.; Mendivil-Palma, I.; Curiel-Alvarez, M.; Mateos, D.; Perez-Landeros, O. Effect of oxidation temperature on the properties of NiOx layers for application in optical sensors. *Thin Solid Films* **2021**, *734*, 138849.
8. Ahmed, A.A.; Hashim, M.R.; Qahtan, T.F.; Rashid, M. Preparation and characteristics study of self-powered and fast response *p*-NiO/n-Si heterojunction photodetector. *Ceram. Int*. **2022**, *48*, 20078–20089.
9. Wang, J.; Li, Q.; Mi, W.; Wang, D.; Xu, M.; Xiao, L.; Zhang, X.; Luan, C.; Zhao, J. Fast response self-powered solar-blind UV photodetector based on NiO/Ga2O3 p-n junction. *Mater. Sci. Semicond. Process*. **2025**, *186*, 109084.
10. Hwang, J.-D.; Cheng, Y.-A. Enhancing the Performance of NiO-Based Metal-Semiconductor-Metal Ultraviolet Photodetectors Using a MgO Capping Layer. *IEEE Sens. J.* **2021,** *21*, 27400–27404.
11. Caglar, M.; Sever, K.; Aktas, S.; Demiroglu A. Improving the electrical performance of NiO based photodiode fabricated by sol-gel process with Al doping. *Sensor Actuat A-Phys* **2023**, *350*, 114099.
12. Pandit, B.; Parida,B., Jang H-S;Heo K. Self-Powered Broadband Photodetector Based on NiO/Si Heterojunction Incorporating Graphene Transparent Conducting Layer. *Nanomaterials* **2024**, *14*, 551 1-11.
13. Wilson, R.L.; Macdonald, T.J.; Lin, C.-T.; Xu, S.; Taylor, A.; Knapp, C.E.; Guldin, S.; McLachlan, M.A.; Carmalt, C.J.; Blackman, C.S. Chemical vapour deposition (CVD) of nickel oxide using the novel nickel dialkylaminoalkoxide precursor [Ni(dmamp')$_2$] (dmamp' = 2-dimethylamino-2-methyl-1-propanolate). *RSC Adv* **2021**, *11*, 22199–22205.
14. Wang, H.; Zhao, Y.; Li, X.; Zhen, Z.; Li, H.; Wang, J.; Tang, M. Effect of Sputtering Temperature on Structure and Optical Properties of NiO Films Fabricated by Magnetron Sputtering. *J. Electron. Mater* **2017**, *46*, 4052–4056.
15. Jamal, M.S.; Shahahmadi, S.A.; Chelvanathan, P.; Alharbi, H.F.; Karim, M.R.; Dar, M.A.; Luqman, M.; Alharthi, N.H.; Al-Harthi, Y.S.; Aminuzzaman, M.; Asim, N.; Sopian, K.; Tiong, S.K.; Amin, N.; Akhtaruzzaman, Md. Effects of growth temperature on the photovoltaic properties of RF sputtered undoped NiO thin films. *Results Phys* **2019**, *14*, 102360.
16. Ahmed, A.A.; Hashim, M.R.; Rashid, M. Effect of RF power on structural, morphological and optical properties of NiO thin films. In Proceedings of AIP Conference, Kelantan, Malaysia, 6 February 2019.

 doi:10.20944/preprints202412.0264.v1

17. Elmassi, S.; Narjis, A.; Nkhaili, L.; Elkissani, E.; Amiri, L.; Drissi, S.; Abali, A.; Bousseta, M.; Outzourhit, A. Effect of annealing on structural, optical and electrical properties of nickel oxide thin films synthesized by the reactive radio frequency sputtering. *Phys. B Condens. Matter* **2022**, *639*, 413980.
18. Abdur, R.; Choudhury, S.; Bashar, M.S.; Hossain, M.R.; Quddus, M.S.; Akhtar, U.S.; Shaikh, M.A.A; Hossain, M. Enhancing perovskite solar cell performance: Investigating the impact of post-annealing on the optoelectrical and structural properties of RF-sputtered NiO films via SCAPS-1D device modeling. *Sol. Energy* **2024**, *271*, 112443.
19. Koushik, D.; Josˇt, M.; Ducˇinskas, A.; Burgess, C.; Zardetto, V.; Weijtens, C.; Verheijen, M.A.; Kessels, W.M.M.; Albrecht, S.; Creatore, M. Plasma-assisted atomic layer deposition of nickel oxide as hole transport layer for hybrid perovskite solar cells. *J. Mater. Chem C* **2019**, *7*, 12532 –12543.
20. Abzieher, T.; Moghadamzadeh, S.; Schackmar, F.; Eggers, H.; Sutterlüti, F.; Farooq, A.; Kojda, D.; Habicht, K.; Schmager, R.; Mertens, A.; Azmi, R.; Klohr, L.; Schwenzer, J.A.; Hetterich, M.; Lemmer, U.; Richards, B.S.; Powalla, M.; Paetzold, U.W. Electronbeam-evaporated nickel oxide hole transport layers for perovskite-based photovoltaics. *Adv. Energy Mater* **2019**, *9*, 1802995.
21. Hasan, M.R.; Xie, T.; Barron, S.C.; Liu, G.; Nguyen, N.V.; Motayed, A.; Rao, M.V.; Debnath, R. Self-powered p-NiO/n-ZnO heterojunction ultraviolet photodetectors fabricated on plastic substrates. *Apl. Mater* **2015**, *3*, 10610.
22. Schroder, D.K. *Semiconductor material and device characterization*, 3rd ed.; Publisher: John Wiley & Sons New Jersey, USA, 2006; p. 187.
23. Grilli, M.L.; Aydogan, S.; Yilmaz, M. A study on non-stoichiometric p-NiOx/n-Si heterojunction diode fabricated by RF sputtering: determination of diode parameters. *Superlattice. Microst* **2016**, *100*, 924–933.
24. Mateos-Anzaldo, D.; Nedev, R.; Perez-Landeros, O.; Curiel-Alvarez, M.; Castillo-Saenz, J.; Arias-Leon, A.; Valdez-Salas, B.; Silva-Vidaurri, L.; Martinez-Guerra, E.; Osorio-Urquizo, E.; Nedev, N. High-performance broadband photodetectors based on sputtered NiOx/n-Si heterojunction diodes. *Optical Materials* **2023**, *145*, 114422.
25. Chen, X.; Ren, F.; Gu, S.; Ye, J. Review of gallium-oxide-based solar-blind ultraviolet photodetectors, *Photon. Res.* **2019**, *7*, 381 –415.
26. Hammadi, O. A.; Khalaf, M. K.; Kadhim, F. J. Fabrication of UV Photodetector from Nickel Oxide Nanoparticles Deposited on Silicon Substrate by Closed-Field Unbalanced Dual Magnetron Sputtering Techniques. *Optical and Quantum Electronics* **2015**, *47* (12), 3805–3813.
27. Ahmed, A. A.; Hashim, M. R.; Qahtan, T. F.; Rashid, M. Multi – Wavelength Photodetectors Based on Porous Spin-Coated and Compact RF-Sputtered NiO Films Grown over Si Substrate: Effect of Surface Morphology. *Optik* **2022**, *255*, 168694–168694.
28. Xu, J.; Cao, R.; Shi, S.; Li, L.; Zhu, K.; Su, Y. Self-Powered Ultraviolet Photodetectors Based on Match like Quasi One-Dimensional N-TiO2/P-NiO Core-Shell Heterojunction Arrays with NiO Layer Sputtered at Different Power. *Journal of Alloys and Compounds* **2022**, *928*, 167126.
29. Enns, Y.; Sergei Timoshnev; Alexey Kazakin; Ksenia Shubina; Uvarov, A.; Vorobyev, A.; Ekaterina Nikitina; Andrey Mizerov; Andreeva, V.; Fedorenko, E.; Koroleva, A.; Evgeniy Zhizhin. Characterization of the P-NiO/N-GaN Heterojunction and Development of Ultraviolet Photodiode. *Materials Science in Semiconductor Processing* **2024**, *181*, 108624–108624.
30. Ma, X.; Tang, L.; Jia, M.; Zhang, Y.; Zuo, W.; Cai, Y.; Li, R.; Yang, L.; Teng, K. S. Ultrahigh Performance UV Photodetector by Inserting an al_2O_3 Nanolayer in NiO/N-Si. *Advanced Electronic Materials* **2024**, *10* (9).